ARTICLE

Check for updates

Calcium availability affects the intrinsic water-use efficiency of temperate forest trees

Filip Oulehle [1,2 ✉], Otmar Urban [2], Karolina Tahovská[3], Tomáš Kolář[2,4], Michal Rybníček[2,4], Ulf Büntgen [2,5,6,7], Jakub Hruška[1,2], Josef Čáslavský [2] & Mirek Trnka [2]

Intrinsic water-use efficiency (iWUE) of trees is an important component of the Earth's coupled carbon and water cycles. The causes and consequences of long-term changes in iWUE are, however, still poorly understood due to the complex interplay between biotic and abiotic factors. Inspired by the role calcium (Ca) plays in plant transpiration, we explore possible linkages between tree ring-derived iWUE and Ca availability in five central European forest sites that were affected by acidic air pollution. We show that increasing iWUE was directly modulated by acid air pollution in conjunction with soil Ca concentration. Responses of iWUE to rising atmospheric CO_2 concentrations accelerated across sites where Ca availability decreased due to soil acidity constraints, regardless of nitrogen and phosphorus availability. The observed association between soil acidity, Ca uptake, and transpiration suggests that Ca biogeochemistry has important, yet unrecognized, implications for the plant physiological upregulation of carbon and water cycles.

[1] Czech Geological Survey, 118 21 Prague, Czech Republic. [2] Global Change Research Institute of the Czech Academy of Sciences, 603 00 Brno, Czech Republic. [3] Department of Ecosystem Biology, Faculty of Science, University of South Bohemia, 370 05 České Budějovice, Czech Republic. [4] Department of Wood Science and Technology, Faculty of Forestry and Wood Technology, Mendel University in Brno, 613 00 Brno, Czech Republic. [5] Department of Geography, University of Cambridge, Cambridge CB2 3EN, UK. [6] Swiss Federal Research Institute (WSL), 8903 Birmensdorf, Switzerland. [7] Department of Geography, Faculty of Science, Masaryk University, 613 00 Brno, Czech Republic. ✉email: filip.oulehle@geology.cz

Calcium (Ca) is the most common alkaline element in the Earth's crust[1]. Ca is relatively easily weathered as a soluble cation from primary and secondary minerals. When liberated, Ca moves readily into the soil solution, where it might be adsorbed onto the soil cation exchange complex, taken up by plants and microorganisms, or leached through the soil profile.

The biogeochemistry of Ca in forest ecosystems is complex because its availability depends on the interplay between supply from atmospheric deposition, cation exchange, mineral weathering, mineralization of soil organic matter, and losses through leaching and biomass accumulation. Anthropogenic influences on the Ca cycle in forests are mainly manifested by Ca removal through tree harvest and soil acidification[2-6]. Although rates of acidic deposition substantially declined in North America and Europe[7], depletion of soil Ca and subsequent mobilization of aluminum (Al) remain a persistent threat to the functioning and productivity of forest ecosystems, especially in areas underlined by acid-sensitive bedrock[8-10]. Differences in litter Ca concentration due to intrinsic differences in species-specific physiology may also cause profound changes in soil acidity and fertility[11]. Ca-rich tree species, like most angiosperms, contain higher foliar Ca, require higher soil pH, and have a faster turnover of soil organic matter than gymnosperm species[12-14].

From a whole-plant perspective, Ca uptake into roots occurs principally by passive movement in the mass flow of soil water driven by the transpiration stream. Thus, tissue Ca supply is often found to be tightly linked to transpiration rates[15]. In plants, calcium acts as a second messenger in regulating various physiological and metabolic processes. Cytosolic Ca^{2+} in leaves, which presents a relatively small fraction compared to the total foliar Ca content, controls leaf gas exchange by regulating stomatal guard cell turgor and thus stomatal opening and closing[16-19]. Stomatal closure is tightly associated with the early activation of anion channels in guard cells. Activation of these channels has been linked with abscisic acid and an enhancement of Ca^{2+} in the cytosol[20,21]. Specifically, the production of non-protein amino acid γ-aminobutyric acid (GABA) is necessary and sufficient to reduce stomatal opening and transpirational water loss, improving water-use efficiency and drought tolerance of plants[22]. GABA production in plants is upregulated by stresses[23], including acidic conditions[24]. In this respect, root activity in obtaining Ca could be potentially indirectly linked to carbon (C) assimilation in the canopy through concurrent regulation of water and carbon fluxes through stomates[25].

The ratio of the minor (^{13}C) to the major (^{12}C) isotopes in plant tissues serves as a valuable natural tracer that can provide important insights into the exchanges of C and water between plants and the atmosphere. The plant tissue ratio of ^{13}C/^{12}C—thereafter referred δ^{13}C (relative deviation from standard)—depends on stomatal conductance to water vapor (g_s) and photosynthesis, which varies according to how plants physiologically respond to changes in their environment. δ^{13}C in tree rings is widely used to infer time-integrated temporal changes of intrinsic water-use efficiency (iWUE), which is defined as the ratio of net photosynthesis (A) to g_s[26-28]:

$$iWUE = \frac{A}{g_s} = \frac{c_a(1 - \frac{c_i}{c_a})}{1.6} \quad (1)$$

where c_i and c_a are the CO_2 intercellular and ambient air concentrations, respectively. As can be seen from Eq. 1, an increase in the atmospheric CO_2 concentration, c_a, will cause a proportional increase in A/g_s of leaves, so long as c_i/c_a remains approximately constant. This means that all else being equal and with stable c_i/c_a, iWUE of terrestrial vegetation is expected to increase in direct proportion to increasing atmospheric CO_2. Evidence from δ^{13}C in tree rings suggests that this situation has been approximately realized[26,29,30]. However, environmental factors distinct from c_a, such as temperature and precipitation[31], plant functional type[32,33], tree size/age[34], nitrogen (N) deposition[35,36], acidic deposition[37,38], have independent effects on net photosynthesis (A) and stomatal conductance (g_s) and, therefore, may modulate the response of iWUE to rising c_a[39].

Given the important, though often neglected, the physiological role of Ca in plants, its soil availability may affect ecosystem water losses through altered tree growth and/or stomatal conductance. At the Hubbard Brook Experimental Forest, Green et al.[40] found that Ca amendment temporarily increased annual evapotranspiration, thus decreasing water runoff from that forest, presumably due to stimulated primary production. Other ecosystem experiments[41,42] observed acidification-induced soil Ca depletion, accompanied by transpiration increases. Higher transpiration could increase the upward movement of dissolved solutes in the xylem and thus enhance Ca delivery from the soil solution to the root surface. Whatever the mechanism of increased transpiration is, one intriguing question remains: "Does calcium availability affect the intrinsic water-use efficiency of trees?".

To answer this question, we sampled wood, foliage, and soil from one broadleaf deciduous and two evergreen conifer species in mixed forests along a gradient of soil acidity and nutrient availability. Our soil chemistry gradient arose from natural environmental effects such as different tree species (one angiosperm *Fagus sylvatica* and two gymnosperms—*Picea abies* and *Abies alba*) combined with different histories of acidic air pollution (Supplementary Table 1).

More specifically, this study seeks to link contemporary ecosystem Ca availability with calculated century-long iWUE changes derived from tree-ring δ^{13}C values to unravel the potential implication of Ca biogeochemistry through effects on tree physiology.

Results

Temporal changes in iWUE. A total of 1448 individual tree-ring derived iWUE estimates reveal a steady increase over the 20th century (Fig. 1). We identified a statistical breakpoint in iWUE in 1991, after which iWUE increased less strongly in European beech, leveled off in Norway spruce and even reversed in Silver fir. These breakpoints coincide with the reversal of sulfur (S) and N deposition and with tree growth recovery across our sites (Supplementary Fig. 1). Due to the contrasting magnitude of iWUE increases amongst individual trees ($F_{74, 1298} = 4.735$, $p < 0.001$), the resulting iWUE change over the study period increased in order: European beech (0.24 ± 0.019 μmol CO_2 mol^{-1} H_2O y^{-1}), Silver fir (0.26 ± 0.032 μmol CO_2 mol^{-1} H_2O y^{-1}), Norway spruce (0.36 ± 0.021 μmol CO_2 mol^{-1} H_2O y^{-1}). To address the influence of atmospheric CO_2 concentration (c_a), climate (precipitation, air temperature, and dryness over the vegetation period), tree growth, and air pollution (S and N deposition) on tree iWUE, we used linear mixed effect (LME) models (see "Methods" for details). A significant positive relationship was indicated between iWUE and environmental factors (c_a, S deposition, tree-ring width index, air temperature, PDSI) and a negative relationship with precipitation (Table 1). LME model results explained 67% of the variance in iWUE (conditional R^2), with 34% of the variance explained by the environmental factors (marginal R^2). Marginal R^2 substantially increases when tree species and sites enter the LME analysis as fixed effects. Norway spruce had significantly higher iWUE by 9.4 ± 2.5 μmol CO_2 mol^{-1} H_2O and Silver fir by 9.9 ± 2.4 μmol CO_2 mol^{-1} H_2O compared to European beech

(Table 1 and Supplementary Fig. 2a). Furthermore, site-specific conditions significantly modulated individual $iWUE$ (Table 1 and Supplementary Fig. 2b), $iWUE$ being lower at less polluted (Novohradské hory) and colder (Orlické hory, Jizerské hory) sites. Complementary to the LME analysis, hierarchical partitioning (HP) indicated that, of the 59% explained variance by the "full" (including species and sites) LME model, c_a account for 43.9%, followed by species (21.3%), dryness index (11.1%), site (10.8%), and S deposition (10.3%).

The linkages across $iWUE$, $diWUE/dc_a$, and ecosystem nutrient biogeochemistry. Due to the high degree of inter-correlated quantitative variables representing soil and foliar chemistry, climate, mean $iWUE$, and $diWUE/dc_a$ (the mean $iWUE$ change with respect to c_a) across our sites and species, we employed principal component analysis (PCA) to identify directions along which the variation in the data is maximal. The first principal direction (Dim 1) represents 46.1% of the variances in our data set. It is associated with variables connecting the acid–base status of soils, foliar Ca content, and $diWUE/dc_a$ (Supplementary Fig. 3). The second principal direction (Dim 2) represents an additional 25.3% of the variance. It is composed of variables connecting mean $iWUE$, soil, and foliage C–N–P stoichiometry, and climate (Supplementary Fig. 3). Thus, $diWUE/dc_a$ and mean $iWUE$ are highly independent of each other and associated with distinct ecosystem properties.

The PCA results were consistent with LME model analysis (Table 1), showing that tree $iWUE$ in broadleaved European beech (high foliar N/P and low C/N, Supplementary Fig. 4) was lower compared to both conifer species. Concurrently, sites with increasing disbalance between soil N and available P (high soil N/P and C/P, such as Orlické hory, Novohradské hory, and Jizerské hory, Supplementary Fig. 3) are those associated with lower mean $iWUE$, again consistent with LME model results (Table 1).

In the $iWUE$ trend, we identified a breakpoint in 1991, which coincided with the reversal of acidic air pollution in central Europe (Supplementary Figure 1). Consequently, the rate of response of $iWUE$ to CO_2 after 1991 weakened or diminished, notably in both conifer species (Fig. 1). Therefore, the resulting $diWUE/dc_a$ over the entire period reflected an apparent rate change of $iWUE$ within the last three decades. The tight association among soil total exchangeable acidity (TEA), Ca availability, and $diWUE/dc_a$ across our environmental gradient, which emerged from PCA, we further demonstrated by regression

analysis. In the combined dataset, soil available Ca explained 69% of the variability in $diWUE/dc_a$ (Fig. 2a), with individual relationships further significant for Norway spruce ($R^2 = 0.84$, $p = 0.028$, $n = 5$ sites) and Silver fir ($R^2 = 0.85$, $p = 0.026$, $n = 5$ sites). Concurrently, soil acidity was significantly inversely related to foliar Ca concentrations, and increasing soil acidity was associated with increasing $diWUE/dc_a$ (Fig. 2b).

Discussion

Our data revealed a complex interaction of rising atmospheric CO_2 concentration, climate, and acidic atmospheric deposition on $iWUE$, consistent with other studies[32,37,38,43,44]. Our analysis emphasizes the pivotal role of sulfur deposition in driving non-linear trends in $iWUE$ of central European temperate forests and provides only limited supporting evidence of the stimulation effect of nitrogen deposition on $iWUE$[35,36,45]. The non-linear temporal increase of $iWUE$ reflected the strong influence of acidic air pollution on stomatal conductance, especially in both conifers. Increases in precipitation acidity likely decreased g_s[18], as tree growth was also suppressed, leading to increased $iWUE$ during the "acid rain" period, as has been consistently shown in areas affected by acidic air pollution worldwide[29,37,38,44,46,47]. Given the high sensitivity of Silver fir $iWUE$[48] and stem growth[49,50] to acidic air pollution, dendrochronological reconstructions may suffer from substantial species-dependent loss of climate sensitivity[51–53] even in areas far from industrial pollution sources. Although our study was not designed to fully resolve the effect of climatic factors on tree physiology, on warmer sites with lower precipitation, the mean $iWUE$ was higher, but over time, $iWUE$ responded positively to PDSI, suggesting conditions favoring higher productivity (A) in wetter years. Furthermore, the design of our study includes mesic regions where annual potential evapotranspiration does not exceed annual precipitation. Thus, the detection of $iWUE$-climate interaction may be confounded by other external and endogenous influences. The combination of tree species and site conditions underscores the intricate interplay between environmental drivers on tree physiology. Specific leaf structure and biochemistry underpinned the intrinsic differences in $iWUE$ among angiosperm and gymnosperm species, being significantly higher in Norway spruce and Silver fir than in European beech[54,55].

The most intriguing result connects the soil acid-base chemistry with the ratio of changes in $iWUE$ in response to increasing ambient CO_2 ($diWUE/dc_a$). As acidic air pollution has declined
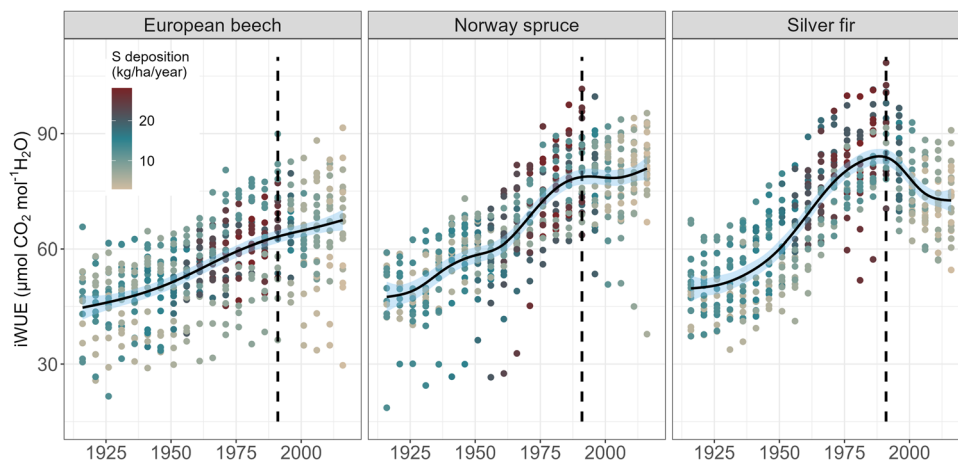

Fig. 1 Species-specific intrinsic water-use efficiency ($iWUE$) trends. Species-specific tree-ring derived $iWUE$ with smoothed (generalized additive model) lines and confidence intervals ($\alpha = 0.95$). Dashed lines indicate significant breakpoints in the data, and point color refers to the estimated sulfur (S) deposition across sites.

Table 1 Linear mixed effect (LME) model and hierarchical partitioning (HP) results.

Predictors	iWUE	iWUE$_{Species}$	iWUE$_{Species+Site}$
Intercept, μmol mol^{-1}	64.664 ± 1.055***	57.581 ± 1.873***	63.231 ± 1.843***
Air CO_2, ppm	0.289 ± 0.014***	0.283 ± 0.015***	0.283 ± 0.015***
S deposition, kg ha^{-1} y^{-1}	1.124 ± 0.079***	0.936 ± 0.141***	0.943 ± 0.142***
N deposition, kg ha^{-1} y^{-1}		0.310 ± 0.194 ns	0.303 ± 0.194 ns
PDSI$_{May-August}$	0.365 ± 0.144*	0.346 ± 0.146*	0.351 ± 0.146*
Precipitation$_{May-August}$, mm	−0.008 ± 0.003**	−0.008 ± 0.003**	−0.008 ± 0.003**
Temperature$_{May-August}$, °C	0.534 ± 0.257*	0.490 ± 0.257 ns	0.494 ± 0.258 ns
Tree-ring$_{index}$	0.023 ± 0.006***	0.021 ± 0.006**	0.021 ± 0.006**
Norway spruce		9.425 ± 2.513***	9.536 ± 2.086***
Silver fir		9.888 ± 2.356***	10.048 ± 1.568***
Jizerské hory			−4.623 ± 2.276*
Novohradské hory			−15.515 ± 2.293***
Orlické hory			−7.784 ± 2.275**
Vysočina			−0.145 ± 2.316 ns
Observations	1448	1448	1448
Marginal R^2	0.34	0.47	0.59
Conditional R^2	0.67	0.68	0.69
AICc	9104	9083	9041
Hierarchical Partitioning	Explained variance (%)$^{Z-score}$		
Air CO_2, ppm	53.5$^{284.46*}$	46.1$^{334.25*}$	43.9$^{315.04*}$
S deposition, kg ha^{-1} y^{-1}	17.8$^{104.96*}$	12.1$^{97.24*}$	10.3$^{74.85*}$
N deposition, kg ha^{-1} y^{-1}			
PDSI$_{May-August}$	17.4$^{95.25*}$	14.6$^{124.53*}$	11.1$^{79.20*}$
Precipitation$_{May-August}$, mm	3.9$^{23.53*}$	5.2$^{41.52*}$	2.2$^{15.76*}$
Temperature$_{May-August}$, °C	6.9$^{39.17*}$		
Tree-ring$_{index}$	0.5$^{2.45*}$	0.4$^{1.9*}$	0.3$^{1.96*}$
Species		21.5$^{113.8*}$	21.3$^{119.76*}$
Site			10.8$^{41.53*}$

LME results for only environmental factors examined (second column), including species as a fixed effect (third column), and including species and site factors as fixed effects (fourth column). Intercept refers to the value when each continuous environmental factor is at its mean value during the study period (1914–2018). The species estimates in the third column refer to the difference from the original intercept represented by European beech. The species and site estimates in the fourth column refer to the difference from the original intercept represented by the European beech at the Beskydy site. Marginal R^2 describes the goodness of the final model fit associated with fixed effects, and conditional R^2 further adds the effect of the random variable (tree ID).
HP results partitioned explained variance among variables retained as significant parameters in the final LME model. A Z-score-based estimate of the "importance" of each predictor is provided by using a randomization test. Asterisks denote parameter significance in the LME and HP models (*$p < 0.05$, **$p < 0.01$, ***$p < 0.001$, and "ns" as not significant; ± denotes standard error).
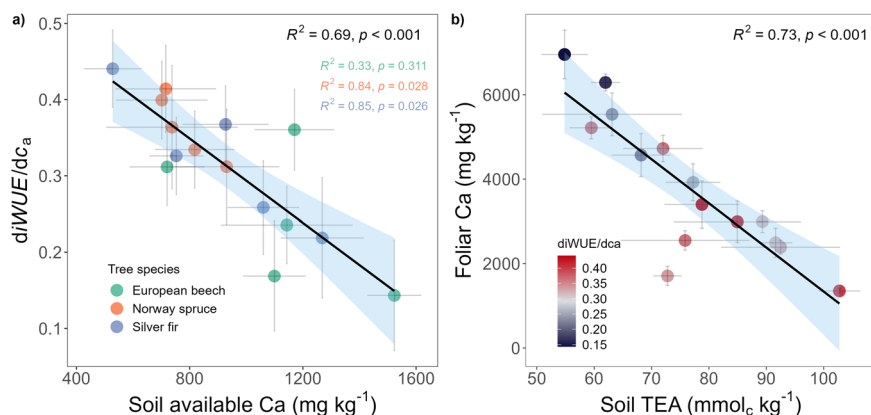

Fig. 2 iWUE response to an increase in ambient CO_2 (d$iWUE$/dc$_a$) related to ecosystem calcium availability. Simple linear regression with confidence intervals ($\alpha = 0.95$) between soil available Ca concentration and d$iWUE$/dc$_a$ ($iWUE$ response to an increase in ambient CO_2, (**a**) and between soil total exchangeable acidity (TEA) and foliar Ca concentration (**b**). Regression coefficients and significance levels in black refer to the combined dataset. Different colors recognize individual species-specific regression results across sites in (**a**), and the point color in the **b** refers to the d$iWUE$/dc$_a$ values. Gray lines indicate standard errors of mean values.

since the late 1980s, $iWUE$ has been adjusting to new levels in compliance with current ecosystem Ca availability. The highest d$iWUE$/dc$_a$ persisted at locations with high soil acidity and low soil Ca availability. Considering that calcium nutrition has improved in conifers and remains unchanged in beech during recent years[56], the observed deacceleration of increasing $iWUE$ in recent decades[43] may be partly related to increased Ca availability for tree uptake.

Since the concentration of Ca in the soil solution is controlled by soil chemistry and diffusion along concentration gradients, it is crucial to recognize the non-linearity of the effects of soil acidity on Ca availability[6]. Ca mobilization is reduced at low soil pH (<4.0), and Al becomes the dominant cation in the soil solution. Concurrently, Ca availability for tree uptake decreases because Al interferes with Ca uptake and root growth[25]. We hypothesize that Ca soil depletion and Al mobilization due to soil acidification

pose significant stress on trees, which upregulates tree water-use efficiency. It has been shown that GABA (γ-aminobutyric acid) is produced under stress conditions[23], including acidic conditions[24]. Our study suggests that the role of the Ca availability, which is constrained by high Al and hydrogen concentrations in acidic soils, appears to be that of fine-tuning stomatal aperture, i.e., capable of adjusting *iWUE* responses under increasing atmospheric CO_2 concentration.

As Ca transport through tissues has been shown to follow apoplastic pathways, tissue Ca supply is often closely linked to transpiration[15]. It is, therefore, likely that higher leaf hydraulic conductance in angiosperms enables higher stomatal conductance and, thus, lower *iWUE* compared to gymnosperms[57]. In the Fernow Experimental Forest (FEF) acidification experiment, Lanning et al.[41] observed an increase in ecosystem evapotranspiration following 25 years of ammonium sulfate addition, which partly contradicts our observations. Authors attributed the increase in vegetation water use to Ca scarcity following soil acidification. Simultaneously, increased aboveground C storage of treated catchment has also been observed, dominating the ecosystem response to long-term N addition[58]. Next, soil pH in our catchments was substantially lower ($pH_{H2O} = 3.69 \pm 0.17$) compared to FEF (pH = 4.02–4.12)[59]. Thus acidity mediated feedback on Ca availability and *iWUE* might be more pronounced in forests under this study.

Calcium-rich tree species modulate the soil environment so that Ca-rich litterfall promotes higher soil pH, exchangeable Ca, soil base saturation, and forest floor turnover[12,60]. Thus, distinct calcium cycling among trees may explain the modulation of the relationship between carbon and water fluxes and contribute to community assembly processes. As such, widespread co-occurrence of beech-spruce-fir in temperate Europe[61] may arise partly from distinct species-dependent Ca biogeochemistry affecting physiological processes. Given the recent growth and competition advances of beech and fir over spruce[62] enhanced water loss through transpiration can be expected[63]. Future research into the integrated role of Ca in water transport processes at tree and ecosystem levels is needed. Furthermore, S deposition in European and North American forests has changed drastically in the past 50 years, implying that pollution may have significantly influenced tree physiology during this period. It also raises the possibility that some observed *iWUE* changes were not caused by climate, at least in areas with acidified soils. We argue that a more holistic approach to the impacts of multiple environmental drivers is needed to correctly interpret existing records and accurately predict future changes in forest ecosystem functioning and productivity in response to global climate and environmental change.

Methods

Study sites and environmental parameters. Five mixed forest sites were selected to represent common temperate forest types across a wide range of nutrient availability conditions in Europe. At each site, mature European beech (*Fagus sylvatica* L.), Norway spruce (*Picea abies* L.), and Silver fir (*Abies alba* Mill.) were sampled to represent a gradient in biological properties (angiosperm vs. gymnosperms) and subsequent nutritional requirements (broadleaf deciduous vs. needle leaf evergreens)[12,64,65]. The forest habitats represent remnants of mixed temperate forest, with uneven-aged structure and non-intensive management. The average age was for beech 110 ± 34 years, spruce 129 ± 28 years, and fir 111 ± 33 years. We further selected individual sites alongside the former acid pollution gradient, with a prerequisite to maintaining a narrow range in elevation and in mean annual air temperature (Supplementary Table 1). Mean growing season precipitation totals range from 320 to 490 mm, with annual precipitation totals between 650 and 1390 mm. Concurrently, annual potential evapotranspiration varied between 505 and 611 mm and is lower than annual precipitation. All sites are underlined by acid-sensitive bedrock (granite, gneiss, mica-schist, sandstone) with a mean CaO rock concentration of 1.0 ± 0.7%. However, in the Beskydy site, CaO concentrations in a mixture of claystone and sandstone (flysch) usually vary between <0.5%

and 10% (source: Czech Geological Survey Lithogeochemic database), which creates heterogenetic soil Ca distribution.

Determination of carbon isotope ratio in tree rings. Wood cores were collected from five trees for each species at each site in 2018. One core per tree was extracted using a Pressler borer (Haglof Company Group, Sweden) at breast height (1.3 m). All cores were sampled parallel to the slope to avoid wood compression. All cores were measured using a VIAS TimeTable device with a measuring length of 78 cm and resolution <0.01 mm (©SCIEM, Vienna, Austria). The obtained tree-ring width (TRW) series were visually synchronized, statistically cross-dated, and additionally corrected for missing and false rings using PAST4 (SCIEM, Vienna, Austria) and COFECHA[66]. To remove non-climatic, age-related growth trends and other non-climatic factors (e.g., competition) from the raw TRW series, we applied cubic smoothing splines with 50% frequency cutoff at 100 years using ARSTAN software[67]. We used this method to preserve inter-annual to multi-decadal growth variations. TRW indices were calculated as residuals between the measured TRW and the corresponding fitted values after applying an adaptive power transformation to minimize end-effect problems. The indexed stand species-specific chronologies were calculated using bi-weight robust means and used for further analysis.

Bulked five-year segments (starting back from the most recent 2014–2018 segment) of 75 precisely dated wood samples were analyzed for their $^{13}C/^{12}C$ isotopic ratios with a continuous-flow mass spectrometer ISOPRIME100 (Isoprime, UK) interfaced with a Vario PYRO cube Elemental Analyzer (Elementar Analysensysteme, Germany) (Supplementary Data 1). The finely homogenized wood samples (Retsch MM200 mill) were weighed (approximate weight of ~1.0 mg), enclosed in tin capsules, and subsequently combusted at 960 °C. Before each set of measurements, the mass spectrometer's ion source was centered and tuned, and tested for stability (standard deviation ≤0.04‰ on ten pulses over three consecutive runs) and linearity (≤0.03‰/nA) over the entire range of expected ion currents obtained from the measurements of test samples. The standard deviation was ≤0.06‰ on five consecutive measurements of the same wood sample. The system was calibrated using certified reference materials with known isotopic ratios from the International Atomic Energy Agency (IAEA) and the United States Geological Survey (USGS). The $\delta^{13}C$ wood values (in ‰) were calculated as the deviation from the Vienna Pee Dee Belemnite (VPDB) standard, according to $\delta^{13}C_{wood} = [(^{13}C/^{12}C_{sample}/^{13}C/^{12}C_{standard}) - 1]*1000$.

Calculation of tree-ring *iWUE*. We calculated $iWUE_{wood}$ from $\delta^{13}C_{wood}$ values based on the known relationship between leaf c_i/c_a and isotopic carbon discrimination ($\Delta^{13}C$)[28,32]. To account for photorespiration and post-photosynthetic fractionation effects, we first calculated c_i based on:

$$c_i = \left(\frac{(\Delta^{13}C - a + f * (\frac{\Gamma^*}{pca}))}{b - a} \right) * c_a, \qquad (2)$$

where a (4.4‰) is the fractionation associated with CO_2 diffusion through stomata[68], f (12‰) is the isotopic fractionation associated with photorespiration[69], pc_a is the partial pressure of atmospheric CO_2 in pascals and b (28‰) denotes fractionation associated with Rubisco carboxylation[69]. c_a is the atmospheric CO_2 concentration in the year of tree-ring formation, and $\Delta^{13}C$ was calculated as follows:

$$\Delta^{13}C = \frac{\delta^{13}C_{atm} - \delta^{13}C_{wood}}{1 + \frac{\delta^{13}C_{wood}}{1000}} \qquad (3)$$

Where $\delta^{13}C_{atm}$ is the carbon isotopic signature of mean atmospheric CO_2 in the years of ring formation. The values of c_a and $\delta^{13}C_{atm}$ were taken from Belmecheri and Lavergne[70] and McCarroll and Loader[71]. Γ^* referred to the Rubisco CO_2 compensation point in the absence of mitochondrial respiration (in pascals) and was calculated as[72]:

$$\Gamma^* = \Gamma_{25}^* * \left(\frac{P_{atm}}{P_0} \right) * e^{\left(\frac{\Delta H_a * ((T+273.15) - 298.15)}{R*(T+273.15)*298.15} \right)}, \qquad (4)$$

where Γ_{25}^* (4.332 Pa) is the Rubisco CO_2 compensation point at 25 °C[73], P_{atm} refers to ambient atmospheric pressure at a given elevation (in pascals), P_0 (101325 Pa) is the atmospheric pressure at sea level, R (8.3145 J mol^{-1} K^{-1}) is the universal gas constant, and T (in °C) is the mean air temperature over the growing season (May–August), and ΔH_a is the activation energy (37,830 J mol^{-1}).

Finally, $iWUE_{wood}$ (in µmol CO_2 mol^{-1} H_2O) was calculated as follows:

$$iWUE_{wood} = (c_a - c_i) * 0.625 \qquad (5)$$

The 0.625 constant accounts for the different diffusivities of H_2O and CO_2[28].

Foliage and soil sampling and analysis. Similarly to wood core retrieval, we randomly selected five trees of each species for foliage sampling at each location (Supplementary Data 2). All foliage samples were collected in August 2018 by tree climbers from the upper third, sun-exposed canopy. Needle samples (restricted to the current year needles) from spruce, fir, and beech leaves were dried at room temperature, homogenized, and analyzed for total organic C and total N by dry

combustion with a CNS elemental analyzer FLASH 2000 (Thermo Scientific, USA). After acid digestion of foliage samples, P concentration was analyzed spectrophotometrically, and Ca concentration by flame atomic absorption spectrophotometry (AAnalyst Perkin Elmer 100, Norwalk, USA).

Soil samples were taken in five replicates for each species at each site at two different soil horizons: forest floor (F + H horizon) and upper mineral soil (A + B horizon). This sampling design resulted in 150 soil samples that were taken within the projection of the tree canopy at a distance of approximately two meters from the tree trunk. Soil samples were air-dried, sieved (mesh size five mm for forest floor and two mm for mineral soil), and analyzed for total organic C and N with a CNS elemental analyzer FALSH 2000. Available P ($P_{available}$) was determined in Mehlich extract by the molybdate blue method[74]. Soil pH was determined in deionized water (1:5 w/v). Using flame atomic absorption spectrophotometry, exchangeable Ca was analyzed in 0.1 M $BaCl_2$ extracts (1:10 w/v). TEA (TEA = Al^{3+} + H^+) was determined by titration of 0.1 M $BaCl_2$ extracts with 0.025 M NaOH solution (to pH of 7.8). We refer to all soil chemistry data as the arithmetic mean of forest floor and mineral soil (Supplementary Data 2). Tree foliage and soil samples were taken independently from trees subjected to wood coring.

Air pollution and climatic variables. To infer historical S and N depositions across our sites, we employed a statistical method based on the temporal coherence between the measured precipitation chemistry and the respective Central European emission rates of SO_2, NO_x, and NH_3 emissions[44,75]. Empirically-based interpolation, taking into account key variables such as altitude, precipitation, and geographical coordinates, enabled the representation of spatial variations in precipitation chemistry (Supplementary Data 1).

Climate data covering the period from the early 1910s to 2018 were derived through interpolation from the three most representative weather stations in the vicinity of each sampling area using locally weighted regressions, including the effect of altitude. All observations of weather variables were tested for outliers and broke through a detailed homogenization sequence, and gaps in missing data were filled[76]. Resulting climate information, i.e., air temperatures, precipitation, and simplified soil water availability indicator (self-calibrated Palmer Drought Severity Index or PDSI[77]), were used to derive environmental variables representing climatic conditions at sites over the vegetation season (May-August) (Supplementary Data 1).

Statistical analysis. To calculate trends in iWUE since 1914, we fit an LME model with *year* as a fixed effect and *tree ID* as a random factor using nlme package[78] in R[79]. We further identified breakpoints in iWUE, deposition, and TRW chronologies using the *segmented* R package[80]. We then used LME models to determine which environmental factors, including atmospheric CO_2 concentration[70], S deposition, N deposition, PDSI, precipitation, air temperature, and standardized TRW, were most affecting long-term iWUE changes. We separately tested LME models with the species and site as fixed factors to assess the importance of local conditions on resulting iWUE trends. Each LME model accounted for temporal autocorrelation, was fit via maximum likelihood, and *tree ID* represented a random factor. The final LME model, having the lowest corrected Akaike information criterion, was selected using the *MuMln* R package[81]. All continuous environmental variables entering LME analysis were standardized to avoid multicollinearity issues. We used hierarchical partitioning (HP) in consecutive analysis to infer the contribution of each predictor to the total explained variance of a final LME model, both independently and in conjunction with the other predictors using *hier.part* R package[82]. A Z-score-based estimate of the "importance" of each predictor is provided by using a randomization test. HP analysis allows the identification of the predictors that explain most variance independently of the others, helping to overcome the problems presented by multicollinearity.

Variation in nutritional and chemical properties of foliage and soils (Supplementary Data 3) was assessed using Principal Component Analysis (PCA). Variables entering the PCA comprised foliage and soil C/N, C/P, and N/P ratios, Ca concentration, soil pH and TEA, and mean temperature and precipitation over the vegetation season. We included calculated mean iWUE and d$iWUE$/dc_a to the environmental variables. R packages *factoextra*[83] were used to summarize and visualize multivariate data with principal components (dimensions). Complementary to our PCA, we used the R package *ggstatsplot*[84] to calculate and visualize the tree-species effect on iWUE. Non-parametric Kruskal–Wallis one-way ANOVA followed by Dunn pairwise comparison of medians was used for data with non-normal distribution. Finally, simple linear regression analysis was employed to accent relationships among d$iWUE$/dc_a, foliage, and soil chemistry (Supplementary Data 4).

Data availability
Measured $\delta^{13}C$ and auxiliary environmental data (Supplementary Data 1) have been deposited at https://doi.org/10.6084/m9.figshare.22496164. All individual soil and foliage chemistry (Supplementary Data 2) have been deposited at https://doi.org/10.6084/m9.figshare.22496161. Supplementary Data 3 can be downloaded here: https://doi.org/10.6084/m9.figshare.22497448. Supplementary Data 4 can be downloaded here: https://doi.org/10.6084/m9.figshare.22792583.

References
1. Wedepohl, K. H. The composition of the continental crust. *Geochim. Cosmochim. Acta* **59**, 1217–1232 (1995).
2. Akselsson, C. et al. Impact of harvest intensity on long-term base cation budgets in Swedish forest soils. *Water Air Soil Pollut. Focus* **7**, 201–210 (2007).
3. Bormann, F. H., Likens, G. E., Fisher, D. W. & Pierce, R. S. Nutrient loss accelerated by clear-cutting of a forest ecosystem. *Science* **159**, 882–884 (1968).
4. Federer, C. A. et al. Long-term depletion of calcium and other nutrients in eastern US forests. *Environ. Manag.* **13**, 593–601 (1989).
5. Leys, B. A. et al. Natural and anthropogenic drivers of calcium depletion in a northern forest during the last millennium. *Proc. Natl. Acad. Sci. USA.* **113**, 6934–6938 (2016).
6. Likens, G. E. et al. The biogeochemistry of calcium at Hubbard Brook. *Biogeochemistry* **41**, 89–173 (1998).
7. Driscoll, C. T. et al. Acidic deposition in the northeastern United States: sources and inputs, ecosystem effects, and management strategies. *Bioscience* **51**, 180–198 (2001).
8. Stoddard, J. L. et al. Regional trends in aquatic recovery from acidification in North America and Europe 1980-95. *Nature* **401**, 575–578 (1999).
9. Likens, G. E., Driscoll, C. T. & Buso, D. C. Long-term effects of acid rain: response and recovery of a forest ecosystem. *Science* **272**, 244–246 (1996).
10. Bauters, M. et al. Increasing calcium scarcity along Afrotropical forest succession. *Nat. Ecol. Evol.* **6**, 1122–1131 (2022).
11. Reich, P. B. The world-wide 'fast–slow' plant economics spectrum: a traits manifesto. *J. Ecol.* **102**, 275–301 (2014).
12. Reich, P. B. et al. Linking litter calcium, earthworms and soil properties: a common garden test with 14 tree species. *Ecol. Lett.* **8**, 811–818 (2005).
13. Sardans, J. et al. Foliar elemental composition of European forest tree species associated with evolutionary traits and present environmental and competitive conditions. *Glob. Ecol. Biogeogr.* **24**, 240–255 (2015).
14. Augusto, L. et al. Influences of evergreen gymnosperm and deciduous angiosperm tree species on the functioning of temperate and boreal forests. *Biol. Rev.* **90**, 444–466 (2015).
15. Gilliham, M. et al. Calcium delivery and storage in plant leaves: exploring the link with water flow. *J. Exp. Bot.* **62**, 2233–2250 (2011).
16. McAinsh, M. R., Clayton, H., Mansfield, T. A. & Hetherington, A. M. Changes in stomatal behavior and guard cell cytosolic free calcium in response to oxidative stress. *Plant Physiol.* **111**, 1031–1042 (1996).
17. McAinsh, M. R., Evans, N. H., Montgomery, L. T. & North, K. A. Calcium signalling in stomatal responses to pollutants. *New Phytol.* **153**, 441–447 (2002).
18. Borer, C. H., Schaberg, P. G. & DeHayes, D. H. Acidic mist reduces foliar membrane-associated calcium and impairs stomatal responsiveness in red spruce. *Tree Physiol.* **25**, 673–680 (2005).
19. DeHayes, D. H., Schaberg, P. G., Hawley, G. J. & Strimbeck, G. R. Acid rain impacts on calcium nutrition and forest health. *Bioscience* **49**, 789–800 (1999).
20. Jezek, M. & Blatt, M. R. The membrane transport system of the guard cell and its integration for stomatal dynamics. *Plant Physiol.* **174**, 487–519 (2017).
21. McAdam, S. A. M. & Brodribb, T. J. The evolution of mechanisms driving the stomatal response to vapor pressure deficit. *Plant Physiol.* **167**, 833–843 (2015).
22. Xu, B. et al. GABA signalling modulates stomatal opening to enhance plant water use efficiency and drought resilience. *Nat. Commun.* **12**, 1952 (2021).
23. Kinnersley, A. M. & Turano, F. J. Gamma aminobutyric acid (GABA) and plant responses to stress. *CRC. Crit. Rev. Plant Sci.* **19**, 479–509 (2000).
24. Ramesh, S. A. et al. GABA signalling modulates plant growth by directly regulating the activity of plant-specific anion transporters. *Nat. Commun.* **6**, 1–10 (2015).
25. McLaughlin, S. B. & Wimmer, R. Tansley review no. 104 calcium physiology and terrestrial ecosystem processes. *New Phytol.* **142**, 373–417 (1999).
26. Frank, D. C. et al. Water-use efficiency and transpiration across European forests during the Anthropocene. *Nat. Clim. Chang.* **5**, 579–583 (2015).
27. Keenan, T. F. et al. Increase in forest water-use efficiency as atmospheric carbon dioxide concentrations rise. *Nature* **499**, 324–327 (2013).
28. Farquhar, G. D., Ehleringer, J. R. & Hubick, K. T. Carbon isotope discrimination and photosynthesis. *Annu. Rev. Plant Physiol. Plant Mol. Biol.* **40**, 503–537 (1989).
29. Saurer, M. et al. Spatial variability and temporal trends in water-use efficiency of European forests. *Glob. Chang. Biol.* **20**, 3700–3712 (2014).
30. Peñuelas, J., Canadell, J. G. & Ogaya, R. Increased water-use efficiency during the 20th century did not translate into enhanced tree growth. *Glob. Ecol. Biogeogr.* **20**, 597–608 (2011).

31. Belmecheri, S. et al. Precipitation alters the CO_2 effect on water-use efficiency of temperate forests. *Glob. Chang. Biol.* **27**, 1560–1571 (2021).

32. Mathias, J. M. & Thomas, R. B. Global tree intrinsic water use efficiency is enhanced by increased atmospheric CO_2 and modulated by climate and plant functional types. *Proc. Natl. Acad. Sci. USA* **118**, e2014286118 (2021).

33. Guerrieri, R. et al. Disentangling the role of photosynthesis and stomatal conductance on rising forest water-use efficiency. *Proc. Natl. Acad. Sci. USA* **116**, 16909–16914 (2019).

34. Marchand, W. et al. Strong overestimation of water-use efficiency responses to rising CO_2 in tree-ring studies. *Glob. Chang. Biol.* **26**, 4538–4558 (2020).

35. Gharun, M. et al. Effect of nitrogen deposition on centennial forest water-use efficiency. *Environ. Res. Lett.* **16** 114036 (2021).

36. Adams, M. A., Buckley, T. N., Binkley, D., Neumann, M. & Turnbull, T. L. CO_2, nitrogen deposition and a discontinuous climate response drive water use efficiency in global forests. *Nat. Commun.* **12**, 5194 (2021).

37. Mathias, J. M. & Thomas, R. B. Disentangling the effects of acidic air pollution, atmospheric CO_2, and climate change on recent growth of red spruce trees in the Central Appalachian Mountains. *Glob. Chang. Biol.* **24**, 3938–3953 (2018).

38. Guerrieri, R. et al. The legacy of enhanced N and S deposition as revealed by the combined analysis of δ13C, δ18O and δ15N in tree rings. *Glob. Chang. Biol* **17**, 1946–1962 (2011).

39. Lavergne, A. et al. Global decadal variability of plant carbon isotope discrimination and its link to gross primary production. *Glob. Chang. Biol.* **28**, 524–541 (2022).

40. Green, M. B. et al. Decreased water flowing from a forest amended with calcium silicate. *Proc. Natl. Acad. Sci. USA* **110**, 5999–6003 (2013).

41. Lanning, M. et al. Intensified vegetation water use under acid deposition. *Sci. Adv.* **5** eaav5168 (2019).

42. Lu, X. et al. Plant acclimation to long-term high nitrogen deposition in an N-rich tropical forest. *Proc. Natl Acad. Sci. USA* **115**, 5187–5192 (2018).

43. Adams, M. A., Buckley, T. N. & Turnbull, T. L. Diminishing CO_2-driven gains in water-use efficiency of global forests. *Nat. Clim. Chang.* **10**, 466–471 (2020).

44. Treml, V. et al. Increasing water-use efficiency mediates effects of atmospheric carbon, sulfur, and nitrogen on growth variability of central European conifers. *Sci. Total Environ.* **838**, 156483 (2022).

45. Leonardi, S. et al. Assessing the effects of nitrogen deposition and climate on carbon isotope discrimination and intrinsic water-use efficiency of angiosperm and conifer trees under rising CO_2 conditions. *Glob. Chang. Biol.* **18**, 2925–2944 (2012).

46. Čada, V. et al. Complex physiological response of Norway spruce to atmospheric pollution—decreased carbon isotope discrimination and unchanged tree biomass increment. *Front. Plant Sci.* **7**, 805 (2016).

47. Kolář, T. et al. Pollution control enhanced spruce growth in the 'Black Triangle' near the Czech-Polish border. *Sci. Total Environ.* **538**, 703–711 (2015).

48. Boettger, T., Haupt, M., Friedrich, M. & Waterhouse, J. S. Reduced climate sensitivity of carbon, oxygen and hydrogen stable isotope ratios in tree-ring cellulose of silver fir (*Abies alba* Mill.) influenced by background SO_2 in Franconia (Germany, Central Europe). *Environ. Pollut.* **185**, 281–294 (2014).

49. Elling, W., Dittmar, C., Pfaffelmoser, K. & Rotzer, T. Dendroecological assessment of the complex causes of decline and recovery of the growth of silver fir (*Abies alba* Mill.) in Southern Germany. *For. Ecol. Manag.* **257**, 1175–1187 (2009).

50. Büntgen, U. et al. Placing unprecedented recent fir growth in a European-wide and Holocene-long context. *Front. Ecol. Environ.* **12**, 100–106 (2014).

51. D'Arrigo, R., Wilson, R., Liepert, B. & Cherubini, P. On the 'Divergence Problem' in Northern Forests: A review of the tree-ring evidence and possible causes. *Glob. Planet. Change* **60**, 289–305 (2008).

52. Büntgen, U. et al. Testing for tree-ring divergence in the European Alps. *Glob. Chang. Biol* **14**, 2443–2453 (2008).

53. Büntgen, U., Kirdyanov, A. V., Krusic, P. J., Shishov, V. V. & Esper, J. Arctic aerosols and the 'Divergence Problem' in dendroclimatology. *Dendrochronologia* **67**, 125837 (2021).

54. Manzoni, S. et al. Hydraulic limits on maximum plant transpiration and the emergence of the safety–efficiency trade-off. *New Phytol.* **198**, 169–178 (2013).

55. Meinzer, F. C. et al. Mapping 'hydroscapes' along the iso- to anisohydric continuum of stomatal regulation of plant water status. *Ecol. Lett.* **19**, 1343–1352 (2016).

56. Jonard, M. et al. Tree mineral nutrition is deteriorating in Europe. *Glob. Chang. Biol.* **21**, 418–430 (2015).

57. Flo, V. et al. Climate and functional traits jointly mediate tree water-use strategies. *New Phytol.* **231**, 617–630 (2021).

58. Eastman, B. A. et al. Altered plant carbon partitioning enhanced forest ecosystem carbon storage after 25 years of nitrogen additions. *New Phytol.* **230**, 1435–1448 (2021).

59. Gilliam, F. S., Walter, C. A., Adams, M. B. & Peterjohn, W. T. Nitrogen (N) dynamics in the mineral soil of a central appalachian hardwood forest during a quarter century of whole-watershed N additions. *Ecosystems* **21**, 1489–1504 (2018).

60. Hobbie, S. E. et al. Tree species effects on decomposition and forest floor dynamics in a common garden. *Ecology* **87**, 2288–2297 (2006).

61. Hilmers, T. et al. The productivity of mixed mountain forests comprised of *Fagus sylvatica*, *Picea abies*, and *Abies alba* across Europe. *Forestry* **92**, 512–522 (2019).

62. Pretzsch, H. et al. Evidence of elevation-specific growth changes of spruce, fir, and beech in european mixed mountain forests during the last three centuries. *Can. J. For. Res.* **50**, 689–703 (2020).

63. Maxwell, T. M., Silva, L. C. R. & Horwath, W. R. Integrating effects of species composition and soil properties to predict shifts in montane forest carbon–water relations. *Proc. Natl Acad. Sci. USA.* **115**, E4219–E4226 (2018).

64. Rothe, A. & Binkley, D. Nutritional interactions in mixed species forests: a synthesis. *Can. J. For. Res.* **31**, 1855–1870 (2011).

65. Augusto, L., Ranger, J., Binkley, D. & Rothe, A. Impact of several common tree species of European temperate forests on soil fertility. *Ann. For. Sci.* **59**, 233–253 (2002).

66. Grissino-Mayer, H. D. Evaluating crossdating accuracy: a manual and tutorial for the computer program cofecha. *Tree-ring Res.* **57**, 205–221 (2001).

67. Cook, E. R. & Krusic, P. J. ARSTAN v. 41d: a Tree-ring Standardization Program Based on Detrending and Autoregressive Time Series Modeling, with Interactive Graphics. (2005).

68. Craig, H. The geochemistry of the stable carbon isotopes. *Geochim. Cosmochim. Acta* **3**, 53–92 (1953).

69. Ubierna, N. & Farquhar, G. D. Advances in measurements and models of photosynthetic carbon isotope discrimination in C3 plants. *Plant. Cell Environ.* **37**, 1494–1498 (2014).

70. Belmecheri, S. & Lavergne, A. Compiled records of atmospheric CO_2 concentrations and stable carbon isotopes to reconstruct climate and derive plant ecophysiological indices from tree rings. *Dendrochronologia* **63**, 125748 (2020).

71. McCarroll, D. & Loader, N. J. Stable isotopes in tree rings. *Quat. Sci. Rev.* **23**, 771–801 (2004).

72. Mathias, J. M. & Hudiburg, T. W. isocalcR: An R package to streamline and standardize stable isotope calculations in ecological research. *Glob. Chang. Biol.* **28**, 7428–7436 (2022).

73. Bernacchi, C. J., Singsaas, E. L., Pimentel, C. Jr, Portis, A. R. & Long, S. P. Improved temperature response functions for models of Rubisco-limited photosynthesis. *Plant. Cell Environ* **24**, 253–259 (2001).

74. Mehlich, A. Mehlich 3 soil test extractant: a modification of Mehlich 2 extractant. *Commun. Soil Sci. Plant Anal.* **15**, 1409–1416 (1984).

75. Oulehle, F. et al. Predicting sulphur and nitrogen deposition using a simple statistical method. *Atmos. Environ.* **140**, 456–468 (2016).

76. Štěpánek, P., Zahradníček, P. & Huth, R. Interpolation techniques used for data quality control and calculation of technical series: an example of a Central European daily time series. *Idojaras* **115**, 87–98 (2011).

77. Wells, N., Goddard, S. & Hayes, M. J. A self-calibrating palmer drought severity index. *J. Clim.* **17**, 2335–2351 (2004).

78. Pinheiro, J., Bates, D. & Team, R. C. nlme: Linear and Nonlinear Mixed Effects Models. (2022).

79. RStudio Team. RStudio: Integrated Development Environment for R. (2022).

80. Muggeo, V. M. R. Interval estimation for the breakpoint in segmented regression: a smoothed score-based approach. *Aust. N. Z. J. Stat.* **59**, 311–322 (2017).

81. Bartoń, K. MuMIn: multi-model inference. (2022).

82. Mac Nally, R. & Walsh, C. J. Hierarchical partitioning public-domain software. *Biodivers. Conserv. 2004 133* **13**, 659–660 (2004).

83. Kassambara, A. & Mundt, F. Extract and Visualize the Results of Multivariate Data Analyses (v. 1.0.7). (2020). Available at: https://github.com/kassambara/factoextra/issues.

84. Patil, I. Visualizations with statistical details: the 'ggstatsplot' approach. *J. Open Source Softw.* **6**, 3167 (2021).

Acknowledgements

Author contributions

F.O. and J.H. designed the study. F.O., O.U., and M.T provided data and interpretation. T.K., M.R., and J.Č. performed the analyses. F.O. and U.B. wrote the paper with input from K.T. All authors contributed to the discussion.

Competing interests

The authors declare no competing interests.